Activity report on the project "*Evaluating photodegradation products of plastic nurdles and their toxicity in Matagorda Bay*"

PIs: Zhanfei Liu, The University of Texas at Austin; Wei Xu, Texas A&M University, College Station, Texas.

Period: June 1, 2025, to February 28, 2026

This report contains three parts: Part I was the manuscript submitted to the Trust during the last report and was just published in *Marine Pollution Bulletin* (see the separate pdf file); Part II is the manuscript led by Dr. Xu's group, out of graduate student Alissa's work; Part III is the complimentary work conducted in Liu group, and the data will be combined to Part II before Alissa's manuscript is submitted to a peer-reviewed journal.

Part I: see the pdf file.

Part II:

Polymer Identity Modulates Toxicity of Photodegraded Plastic Leachates in Marine Medaka (*Oryzias melastigma*)

Alissa Richbourg[a], Xudan Yang[b], Kaitlin Garcia[c], Lora Schell[c], Kimberly Gaston[c], Xiangtao Jiang[b], Kadee Loyd[b], Jordan Ciscob, Frauke Seemann[a], Zhanfei Liu[b,*], Wei Xu[c,*]

[a]Department of Life Sciences, Texas A&M University-Corpus Christi, Corpus Christi, Texas, USA;
[b]Department of Marine Science, The University of Texas at Austin-Marine Science Institute, Port Aransas, Texas, USA;
[c]Department of Veterinary Physiology and Pharmacology, Texas A&M University College of Veterinary and Biomedical Sciences, College Station, Texas, USA.

[*]*Corresponding author:
Zhanfei Liu, 750 Channel View Drive, Port Aransas, TX 78373. E-mail: zhanfei.liu@utexas.edu;
Wei Xu, 402 Raymond Stotzer Pkwy, College Station, Texas, 77843. E-mail: wxu1@tamu.edu

Abstract

Text.

Text.

Keywords: Photodegradation, plastic leachates, microplastic toxicity, marine medaka

1. Introduction

Plastic is a commonly used material for many industries and consumers, with long-lasting properties and plasticity. As a result of its wide-ranging applications, the accumulation of plastics globally has become one of the most prominent issues facing both marine and human health in the last several decades (Madiraju et al., 2024). Estimates predict that by 2030, 90 million metric tons of plastic debris will enter the world's oceans every year under current disposal rates (Borrelle et al., 2020). Macroplastics (> 5mm) have been shown to pose a severe threat to marine life through ingestion, entanglement, and suffocation, causing physical damage and potentially mortality (Chapron et al., 2018; Gregory 2009). Macroplastics are also subject to physical changes such as fragmentation, photodegradation, and biodegradation once they have entered marine environments (Gewert et al., 2015). These chemical and physical processes break down manufactured plastics into micro and nanosized particles, resulting in the release of plastic additives, polymers, and monomers into aquatic environments (Andrady 2022).

Photodegradation is a major contributor to the breakdown of plastics in ocean environments, a process by which disposed plastic products are degraded by harsh UV radiation from the sun and may release compounds and chemicals with unknown toxicities into the ocean (Delre et al., 2023). The presence of these chemicals, known as plastic leachates, can pose a large threat to marine environments, as it is not easy to observe, identify, or track their abundance (Tuuri & Leterme, 2023). The potential toxicological effects of photodegradation and the formation of plastic leachates remain underexplored, especially regarding how these leachates may disrupt biological systems and whether these impacts vary across polymer types. Exposure to plastic leachates has been shown to induce toxicity and increase mortality in *Caenorhabditis elegans* (Reyes & Medina, 2024), the sea cucumber *Apostichopus japonicus* (Wang et al., 2023), and the barnacle *Amphibalanus Amphitrite*. The effects of plastic leachates

on critical biological pathways, including reactive oxygen species (ROS) regulation, oxidative stress response, and inflammatory signaling, are still being investigated. Exposure of *Donax faba*, a marine clam, to PS leachates from pharmaceutical bottles has been shown to elevate ROS levels and decrease the activity of superoxide dismutase (*sod*) and catalase (*cat*) genes (Sunil et al., 2023). These genes play an essential role in regulating ROS levels and the antioxidant system (Huang et al., 2023). In marine medaka *(Oryzias melastigma)* embryos, exposure to simulated seawater leachates has been shown to inhibit the expression of cyclooxygenase-2 (*cox-2*), associated with the inflammatory response of the cardiovascular system, and interleukin-1 beta (*il-1ß*), an inflammatory response initiator (Qiu et al., 2022). However, few studies have done a comprehensive assessment of how plastic leachates affect marine organisms across multiple molecular pathways to better understand the mechanisms behind plastic leachate toxicity.

Model organisms are used as tools to evaluate biological responses to toxicant exposure, providing insights into how other organisms, including humans, may be affected (Aschner et al., 2025). The marine medaka (*O. melastigma)* is a small marine fish with emerging use in marine pollution and toxicology studies (Horie and Takahashi 2021), due to its small size, short generation time, distinct sexual dimorphism, clear embryos, and ability to tolerate varying salinities (Dong et al., 2014). Traditionally, fish model species such as zebrafish (*Danio rerio*) and Japanese rice fish (*Oryzias latipes*) are used in toxicology studies due to their well-characterized genomes and ease of laboratory use. However, these species are restricted to freshwater environments, limiting their applicability for marine studies. Marine medaka provide a valuable alternative, offering comparable traits to zebrafish and Japanese medaka, while also being relevant to marine and estuarine toxicology studies (Dong et al., 2014).

To further investigate the toxicological impacts of photodegraded plastic leachates on aquatic organisms, nurdles of five of the most abundant types of plastic pollutants in the environment, polycarbonate (PC), polyethylene terephthalate (PET), polystyrene (PS), polypropylene (PP), and high-density polyethylene (HDPE or PE) (Medina Faull et al., 2024), were photodegraded using UV radiation for 8 weeks to generate plastic leachates at known concentrations. This study assessed the effects of plastic leachate exposure on the development, hatching, and survival of marine medaka embryos during critical developmental stages, as well as evaluated the health and survival of adult marine medaka exposed to plastic leachates by investigating changes in organ structures and gene expression levels. The mechanisms of toxicity and evaluations of toxicity across polymer types were explored, providing insight into the inherent toxicity of the polymers, independent of additives.

2. Materials and Methods

2.1 Fish maintenance

Adult marine medaka (3 months old) were kept in 2.5-gallon tanks with 15 males and 15 females. Tanks were maintained at 28–30 ppt and monitored daily for embryos. Collected embryos were rinsed and cultured in glass Petri dishes containing 900 mL filtered artificial seawater, 100 mL RO water, and 20 drops of methylene blue. Embryos were examined under a dissecting microscope (Olympus CKX53) to identify those at 24 hours post-fertilization using published developmental standards for *Oryzias latipes*, which closely match marine medaka (Murata et al., 2019). Embryos were maintained in an incubator at 28 °C under a 12:12 light–dark cycle.

2.2. Generation of plastic leachates

Pure PC, PET, PS, PP, and HDPE plastic nurdles were purchased from a commercial vendor (Polyplastics on Amazon), and their composition was verified using Fourier Transform Infrared Spectroscopy (FTIR). Plastic nurdles were washed and sterilized prior to UV exposure. For the photooxidation experiment, light and dark treatments were conducted in triplicate. For the light treatment, 1 g of clean plastic nurdles was added to 110 mL of artificial seawater (InstantOcean®, 33 ppt) in a sterile 120 mL quartz bottle. The solution was photodegraded in an Atlas XLS+ solar simulator maintained at 33 ± 2 °C for 8 weeks and equipped with a filter-Q for artificial natural sunlight. The simulator induced an average irradiation of 5000 μmol photons/m^2/s, with 8 weeks equivalent to 3 years of natural diel sunlight. The dark treatment used the same setup with amber glass bottles kept in a closed box to determine whether UV exposure caused any changes. Samples were shaken daily for 10 seconds and opened briefly to balance pressure.

Light-treatment samples were collected at week 8, and nurdles were removed by vacuum filtration with a 0.7 µm glass fiber filter. Filtrates were analyzed using a total organic carbon analyzer (Shimadzu TOC-V) to determine final DOC concentrations (Table 1). An aliquot of filtrate (90 mL) from each plastic type was used for DOC analysis and toxicity assessments. DOC concentrations in bottles containing PC, PET, PS, PP, and PE increased during the 8-week photodegradation period. Light treatment increased DOC concentrations significantly more than dark treatment, indicating that chemicals and/or polymers leached into solution during photodegradation.

Filtrates were diluted with control seawater (28–30 ppt) to prepare three concentrations (0.1, 0.5, and 5 ppm) for each plastic type (PC, PE, PET, PS, and PP) for marine medaka embryo exposures. Control water consisted of a 1:1 mixture of filtered artificial seawater (30 ppt) and seawater from breeding adult tanks. Determining environmentally relevant concentrations of plastic leachates is difficult due to the vast number of chemicals, additives, and compounds that may be released as plastics are photodegraded. Previous studies have used plastic leachate concentrations ranging from 0.01 mg/L to 8000 mg/L (Sources), as there is no clear consensus regarding how to generate and use plastic leachates in toxicity assessments. Therefore, three concentrations were chosen to represent low (0.1 ppm), high (0.5 ppm), and very high (5.0 ppm) exposure levels to assess whether toxicity effects were concentration dependent.

Table 1. Final DOC concentrations (mg/L) measured after an 8-week photodegradation period

Polymer	Treatment Length	Final DOC Concentration (mg/L)
PE	8-weeks	72.39
PET	8-weeks	26.30
PP	8-weeks	127.17
PS	8-weeks	20.00
PC	8-weeks	10.86

2.3 Experimental design and developmental analysis

To assess early development in marine medaka, developmental experiments were conducted with PC, PET, PS, PP, and PE leachates at three concentrations (0.1, 0.5, and 5 ppm). Embryos 24 hours post-fertilization were randomly assigned to treatment and control groups, with 5 replicates per group and 5 embryos per replicate (25 embryos total; Fig. 2). Embryo development was monitored daily for 14 days, and stage, mortality, and hatching status were recorded. Deformities before and after hatching were noted and photographed using a compound microscope (Olympus CKX53). Endpoint mortality and hatching rates were calculated on day 14 for each replicate. Kaplan–Meier survival and hatching curves were generated to analyze trends over the exposure period. Heart rate was measured on days 4, 6, 8, and 10 by randomly selecting 5 embryos from each treatment group and counting heartbeats over 20 seconds (Huang et al., 2011).

Adult marine medaka (3 months old) were randomly assigned to 5 L tanks. The adult exposure experiment included four treatments: PE 0.1 ppm, PE 0.5 ppm, PC 0.1 ppm, and a control with artificial seawater (28–30 ppt). Each treatment included two tanks, one with 20 females and one with 20 males. Adults were observed for 16 days, and mortality, deformities, and unusual behavior were recorded. Approximately 10 adults from each tank were collected at the end of the study for genetic analysis, and 10 for histological analysis.

2.4 Histological analysis

Male and female adult marine medaka exposed to PC and PE leachates for 16 days were fixed in paraformaldehyde for histological examinations. Samples were embedded in paraffin wax, and longitudinal 4-μm sections were cut using a rotary microtome (Leica RM2125 RTS, Leica Biosystems, Nussloch, Germany). Sections were stained with hematoxylin and eosin (H&E), and photos of the liver and gill tissues were taken to compare the morphologies of the treatment and

control samples. Images were assigned a unique identifier to ensure that reviewers were blind to treatment groups. Four trained observers independently scored the photos on a semi-quantitative 0–3 scale (0 = normal; 1 = mild; 2 = moderate; 3 = severe) based on lesion severity, including hepatocyte distribution, vacuolation, presence of lipofuscin granules, and liver color. Up to 14 slides were evaluated per fish, and scores were averaged across observers to generate a single composite score per fish sample.

Immunofluorescence (IF) was performed using a Ki-67 antibody (Rabbit × Human polyclonal, Cat# NB110-90592, Novus Biologicals, Centennial, CO), which has previously been shown to work in fish (Mealiea et al., 2020). The paraffin-embedded slides were incubated at 40˚C overnight. Following the complete deparaffinization by xylene and rehydration by serially diluted ethanol, the slides were submerged in citrate buffer (10 mM tri-sodium citrate with 0.05% Tween-20, pH 6.0) and incubated in a steamer for 20 minutes to retrieve the antigens from the tissues. Thoroughly washed by PBS, the slides were incubated with a 1:200 diluted Ki-67 primary antibody in PBST (PBS + 0.05% Tween-20) containing 10% goat serum at 4˚C overnight. Donkey × Rabbit IgG (H+L) Alexa Fluor™ 488 secondary antibody (Thermo Fisher Scientific, Cat# A-21206) was used in a dilution of 1:200 with PBST and incubated with the slides stained with DAPI prior to microscopic observation. The fluorescent imaging was performed with Nikon TS2-FL (Nikon USA, Melville, NY) with a DS-Fi3 high-definition color microscope camera equipped with a 5.9-megapixel CMOS image sensor (Nikon USA).

IF images were analyzed using ImageJ (2.16.0/1.54p) to determine the percentage of proliferating cells relative to the total number of cells present in the gill tissues. Results for each image were standardized by dividing the number of Ki-67 fluorescent cells present by the total

area of cells stained with DAPI, and then multiplying by 100 to obtain the percentage of proliferating cells in the gill tissue samples.

2.5 RT-qPCR analysis of target genes

The genetic response of male and female adult marine medaka exposed to PC and PE leachates for 16 days was evaluated using real-time quantitative polymerase chain reaction (RT-qPCR). The male and female control groups received no treatment. Genes related to oxidative stress, inflammatory response, xenobiotic metabolism, and the immune system were chosen to determine the genetic response of adult marine medaka to PC and PE leachate exposure (Supplementary Data Table S1). Total RNA from each sample was isolated using the Trizol method, and cDNA was synthesized using the Promega Reverse Transcriptase kit (Promega Corporation, Madison, USA). RT-qPCR was performed using the Sybr Green method, and the data were calculated using the $2^{-\Delta\Delta CT}$ method (Livak and Schmittgen, 2001). CT values were normalized against the housekeeping gene, 18S rRNA.

2.8 Statistical analysis

Data were analyzed using R Studio (2023.12.1+402) and Microsoft Excel (2024). Mortality and hatching data from all developmental studies were evaluated using Kaplan–Meier survival analysis to estimate survival and hatching probabilities for each treatment over time, and pairwise comparisons were performed using a log-rank test at the 0.5 significance level.

Differences in embryo heart rates across treatments and days were analyzed using a linear mixed-effects model (LME) with treatment, day, and their interaction as fixed effects and replicate as a random effect. A likelihood ratio test compared a model assuming equal variances across treatments with one allowing treatment-specific variances. The variance-heterogeneous model was a better fit for PE, PC, PET, and PS ($p < 0.0001$, $p = 0.0374$, $p = 0.0003$, and $p =$

0.0311), while the equal-variance model fit PP better ($p = 0.2494$). Normality was assessed using a Q–Q plot and histogram, and homoscedasticity by plotting residuals vs. fitted values. Random effects showed no pattern, supporting independence. Estimated marginal means (EMMs) and 95% confidence intervals were calculated using the containment method. Pairwise comparisons between treatments on each day used Tukey-adjusted contrasts.

Deformity results, IF cell proliferation results, and relative gene expression data for PE treatments were evaluated using a one-way ANOVA followed by Tukey's HSD test. Relative gene expression for PC was assessed using Welch's t-test. Outliers were identified using Grubbs' test and removed. Unless noted otherwise, data are expressed as means ± standard error. For all statistical tests, differences were considered significant at $*P < 0.05$, $**P < 0.01$, and $***P < 0.0001$.

3. Results

3.1 Embryo mortality and hatching rates

Kaplan-Meier survival curves showed that all plastic types, excluding PE, had significantly faster mortality probabilities than the control in at least one treatment group. Exposure to PC 0.1 ppm resulted in a 28% higher mortality than the control ($p = 0.01662$; Fig. 2A). Exposure to PET 5.0 ppm resulted in a 32% higher mortality than the control group ($p = 0.0087$; Fig. 2B). Exposure to PS 5.0 ppm treatment group also resulted in a 28% higher mortality than the control group ($p = 0.0100$; Fig. 2C). Exposure to PP 0.5 ppm resulted in a 16% higher mortality than in the control group ($p = 0.039$; Fig. 2D). For PE, both the control and treatment groups exhibited very low mortality overall (Fig. 2E).

Fig. 2 Percent survival of embryos exposed to PC (**A**), PET (**B**), PS (**C**), PP (**D**), and PE (**E**) leachates at different concentrations across a 14-day exposure (n = 25). Data was expressed as a Kaplan-Meier curve, and significance was evaluated using a log-rank test at the 0.05 significance level. Asterisk (*) denotes significance compared to the control (* < 0.05, ** < 0.01).

Our hatching curve analysis showed that exposure to PC 0.1 ppm, PET 5.0 ppm, PP 0.5 ppm, and PP 5.0 ppm resulted in significantly slower hatching rates (Fig. 3). Hatching rates were significantly slower than the control in the PC 0.1 ppm treatment group ($p = 0.054$, Fig. 3A), as well as the PET 5.0 ppm treatment group ($p = 0.02$; Fig. 3B). Hatching rates were also significantly slower than the control in the PP 0.5 ppm treatment group ($p = 0.0404$; Fig. 3D) and in the PP 5.0 ppm treatment group ($p = 0.0105$; Fig. 3D). The rates at which hatching occurred in the PS treatment groups were not significantly different (Fig. 19).

Fig. 3 Cumulative hatching rates of embryos exposed to PC (**A**), PET (**B**), PS (**C**), PP (**D**), and PE (**E**) leachates at different concentrations across a 14-day exposure (n = 25). Data was expressed as a Kaplan-Meier curve, and significance was evaluated using a log-rank test at the 0.05 significance level. Asterisk (*) denotes significance compared to the control (* < 0.05, ** < 0.01).

3.2 Developmental analysis

Exposure to PET leachates induced developmental deformities at all three treatment concentrations. The PET 0.5 ppm treatment group resulted in the highest rate of deformity at 20% ± 6.32% and was significantly higher compared to the control ($p = 0.0278$, Fig. 4B). Deformities consisted of spinal deformations, including curved, bent, and kinked tails that inhibited the larvae's locomotive abilities (Fig. 4A). In all cases of curved spines, swimming ability was inhibited completely, and those with kinked or bent tails showed little to no swimming ability. Exposure to PC 0.1 ppm and PC 5.0 ppm leachates also induced developmental deformities. No deformities were observed in the PC 0.5 ppm treatment group. The highest deformity rate, which consisted of both spinal deformations and incomplete development of the upper jaw (Fig. 4A), was seen in the PC 0.1 ppm treatment group, with a rate of 12% ± 8.00% (Fig. 4C). Spinal deformations included bent and curved tails that inhibited locomotion. Upper jaw deformities did not impact immediate survival or locomotion. Deformities were not observed in any of the PS, PP, or PE treatment or control groups.

Fig. 4 Morphological changes in larvae exposed to PET and PC leachates (**A**). SD = spinal deformity; JD = jaw deformity. Scale bar: 1 mm. Effects of PET (**B**) and PC (**C**) leachates on developmental deformities across five replicates (n = 5; 5 embryos per replicate, 25 per treatment). Data shown as means ± SE. Asterisks indicate significance vs. control (* < 0.05, ** < 0.01, *** < 0.001).

3.3 Heart rate analysis

Exposure to plastic leachates significantly reduced heart rates on at least one day for all treatments (PC, PET, PS, PP, PE) when compared to their respective control groups. PC leachates reduced heart rates only on day 6. Heart rates were, on average, 21.6 bpm slower in the PC 5.0 ppm exposure than the control on day 6 ($p = 0.0400$; Fig. 5A). PET leachates reduced heart rates on days 4 and 6. Exposure to PET 5.0 ppm reduced heart rates by 31.8 bpm on average relative to the control on day 4 ($p = 0.0067$; Fig. 5B). On day 6, heart rates were on average 47.4 bpm slower in the PET 0.1 ppm exposure ($p = 0.0002$), 36.0 bpm slower in the PET 0.5 ppm exposure ($p = 0.0173$), and 31.2 bpm lower in the PET 5.0 ppm exposure ($p = 0.0080$). PS leachates reduced heart rates on days 4, 6, and 8 (Fig. 5C). Heart rates were on average 33.6 bpm slower in the PS 0.1 ppm group on day 4 ($p = 0.0021$) and 31.2 bpm slower in the 5.0 ppm group ($p = 0.0028$). On day 6, the 5.0 ppm group was on average 27.0 bpm slower ($p = 0.0122$). On day 8, heart rates were on average 27.0 bpm slower in the 0.5 ppm group ($p = 0.0293$) and 40.2 bpm slower in the 5.0 ppm group ($p = 0.0001$; Fig. 5C). Similarly to PC, PP leachates reduced heart rates only on day 6 (Fig. 5D). Heart rates were on average 29.4 bpm slower in the PP 0.5 ppm exposure ($p = 0.0381$) and 49.2 bpm slower in the PP 5.0 ppm exposure ($p = 0.0001$) on day 6. PE leachate exposure reduced heart rates on days 6, 8, and 10. On day 6, heart rates were on average 21.0 bpm slower in the PE 5.0 ppm exposure relative to the control ($p =$

283 0.0289), 21.6 bpm slower on day 8 (p = 0.0233), and 21.6 bpm slower on day 10 (p = 0.0233;

284 Fig. 5E).

285 **Fig. 5** Effects of PC (**A**), PET (**B**), PS (**C**), PP (**D**), and PE (**E**) leachates on heart rate at three
286 concentrations. Heart rates expressed as the average of 5 replicates (n = 5). Data expressed as
287 estimated marginal means ± 95% CIs. Asterisk (*) denotes significance compared to the
288 control (* < 0.05, ** < 0.01, *** <0.001).

289 *3.4 Histological analysis of adult marine medaka*

290 Gill morphology showed no observable differences between treatment and control

291 groups, so pathological scoring was not performed. Variations in liver morphology were evident

292 between the treatment and control groups, although average histological lesion scores were not

significant between groups ($F(3, 21) = 2.315$, $p = 0.105$). All treatment groups exhibited higher average lesion scores than the control group, showing evidence of hepatocellular vacuolation and excess accumulation of lipofuscin granules (Fig. 6).

IF staining in the gill tissues revealed significant differences in average cell proliferation between treatment groups ($F(3, 20) = 3.494$, $p = 0.035$). Average cell proliferation was significantly higher in the PC 0.1 ppm treatment group (0.20 ± 0.02) than in the control group (0.13 ± 0.02, $p = 0.047$, Fig. 7). Average cell proliferation was also increased compared to the control in the PE 0.1 and PE 0.5 ppm treatment groups, although not significantly so.

Fig. 6 (**A**) Pathological scoring criteria used to evaluate liver damage in adult marine medaka. Level 0: normal; Level 1: mild damage; Level 2: moderate damage; Level 3: severe damage. Arrows indicate hepatocellular vacuolation, and circles highlight lipofuscin granule accumulation. Scale bar = 50 μm. (**B**) Mean histological lesion scores for each treatment group (n = 6–7). Data expressed as means ± SE.

Fig. 7 (**A–D**) Immunofluorescent staining of gill tissue in adult marine medaka using a Ki-67 antibody (green) to identify proliferating cells and a DAPI counterstain (blue) to label nuclei. Representative images are shown for the control (**A**), PE 0.1 ppm (**B**), PE 0.5 ppm (**C**), and PC 0.1 ppm (**D**) groups. Scale bar = 100 μm. (**E**) Mean cell proliferation (%) observed in each treatment group (n = 6). Data expressed as mean ± SE. Asterisks indicate significant differences compared with the control (*P < 0.05, **P < 0.01, ***P < 0.001).

3.5 Effect of PC and PE leachates on gene expression levels of adult marine medaka

Exposure of adult marine medaka males to PC leachates induced widespread downregulation of several genes across multiple pathways, while females showed targeted upregulation of detoxification and immune response genes (Fig. 7). In males exposed to PC 0.1 ppm, *sod* expression was downregulated 124.9-fold relative to the control ($p < 0.0001$), and glutathione peroxidase (*gpx)* expression was downregulated 3.4-fold relative to the control ($p = 0.002$). CYP1A1 expression was also downregulated 4.7-fold relative to the control ($p = 0.001$), and there was no significant difference observed in aryl hydrocarbon receptor gene (*ahr)* expression between the treatment and control ($p = 0.225$). The expression of *il-1β* was

downregulated 4.6-fold relative to the control ($p = 0.029$), and *cox-2* was downregulated 5.2-fold relative to the control ($p = 0.004$). The expression of *c3* was 1.9-fold lower than the control but was not significantly different ($p = 0.139$). In females exposed to PC 0.1 ppm, *sod* expression was 2.1-fold higher than the control, but not significantly different ($p = 0.156$). The expression of *gpx*, *ahr*, *c3*, and *cox-2* was unchanged relative to the control (Fig. 7). *Cyp1a1* expression was upregulated 3-fold relative to the control ($p = 0.045$), and *il-1β* expression was upregulated 2-fold relative to the control ($p = 0.027$).

Exposure of females to PE leachates induced significant changes to the detoxification and immune response genes, while males showed severe downregulation of only the antioxidant defense genes (Fig. 7). In males exposed to PE 0.1 ppm and PE 0.5 ppm, *sod* expression was downregulated 91.1-fold ($p = 0.001$) and 17.6-fold ($p = 0.005$), respectively. *Gpx* expression was also downregulated 2.1-fold (0.050) and 3.2-fold (0.004) in the PE 0.1 ppm and PE 0.5 ppm treatment groups, respectively. No significant differences in expression were observed in *ahr*, *cyp1a1*, *il-1β*, *c3*, and *cox-2* compared to the control. In contrast, females exposed to PE 0.1 ppm and PE 0.5 ppm showed no significant differences in *sod* or *gpx* expression. *Ahr* expression in the PE 0.5 ppm treatment group was upregulated 2.4-fold relative to the control ($p = 0.028$). *cyp1a1* expression in the PE 0.1 ppm and 0.5 ppm treatment groups was downregulated 7.9-fold (0.005) and 311.6-fold ($p < 0.001$), respectively. In the PE 0.1 ppm treatment group, *il-1β*

expression was upregulated 4.5-fold ($p = 0.001$) relative to the control. *C3* and *cox-2* expression in females exposed to PE leachates remained unchanged from the controls.

Fig. 8 (**A**) Heatmap of gene expression in adult marine medaka exposed to PE and PC leachates. Colors represent log_2 fold changes relative to controls (blue = downregulated, white = no change, red = upregulated). n = 3–5. (**B**) Relative expression levels of key genes affected by PE and PC leachates. Asterisk (*) denotes significance compared to the control (* < 0.05, ** < 0.01, *** <0.001).

4. Discussion

4.1 Effects of plastic leachates on embryo mortality

Survival probability for marine medaka embryos was significantly reduced in at least one treatment group for all polymer types except PE. Mortality was greatest in the 5.0 ppm PET and 5.0 ppm PS treatment groups, suggesting a potential dose-response effect. Our findings are supported by previous studies showing that plastic leachates can induce significant mortality in fish embryos. Plastic leachates from agricultural mulching films led to significant mortality in zebrafish (*D. rerio*) embryos when exposed to high concentrations (Li et al., 2023). Although their exposure concentrations (6–8 g/L) were far higher than those in the present study, their results similarly demonstrate that both high and relatively low concentrations of leachates can impair embryo survival. Additionally, our results are consistent with studies showing that UV-weathered plastics increase mortality in aquatic invertebrates, such as the copepod *Nitocra spinipes* (Gewert et al., 2021), further supporting the conclusion that plastic leachates may induce mortality in a variety of taxa.

Our results suggest that mortality occurred more rapidly and severely under exposure to PC and PET leachates, whereas PS induced moderate effects, and PP and PE leachates induced weaker effects. Recent studies comparing toxicities among different plastic types are not fully supported by our findings. Exposure to PS and PET exhibited relatively low toxicity in the copepod *Nitocra spinipes*, while PP induced relatively high toxicity (Gewert et al., 2021). These results conflict with our conclusions that PS and PET induced significant mortality, while PP exhibited lower mortality rates overall. These differences may reflect species-specific susceptibility between copepods and marine medaka, as well as potential variation in the chemical composition of the plastics used. The plastic leachates used in the present study consist

of photodegradation products that include particles, polymers, and monomers of varying sizes. This variation may help explain some of the discrepancies in toxicities when comparing our results to those of studies assessing the toxicity of single-sized plastic particles.

4.2 Effects of plastic leachates on embryo hatching success

Hatching success is an essential endpoint in toxicity testing because it provides insight into both developmental progression and overall embryo health (Suter II et al., 1987). In this study, cumulative hatching was significantly delayed in the PC 0.1 ppm, PET 5.0 ppm, and both the PP 0.5 ppm and PP 5.0 ppm treatment groups compared to controls. Although not statistically significant, most other treatment groups exhibited 8–16% lower hatching rates than the controls, suggesting a consistent trend toward delayed hatching across polymers. Although relatively few studies have examined the embryotoxicity of plastic leachates, our results are consistent with prior findings. Hatching rates were not affected in marine medaka exposed to degraded PVC leachates, but hatching times were significantly decreased relative to the controls (Xia et al., 2022). Slower hatching has important ecological implications, as it can decrease survival and recruitment by prolonging the vulnerable embryonic stage and delaying the transition to free-feeding larvae (Lee et al., 2018).

4.3 Effects of plastic leachates on embryo development

Developmental deformations were observed in all PET treatment groups, with the 0.5 ppm treatment group exhibiting the highest rate of deformity at 20% (Fig. 4B). Deformities were also observed in the 0.1 and 5.0 ppm PC treatment groups. Both PET and PC leachate exposure resulted in spinal deformations, including curved or bent spines, as well as kinked tails. These malformations resulted in a partial or complete reduction in locomotive ability for the affected

larvae, which may have serious implications for long-term survivability (Sfakianakis et al., 2015). Additionally, PC exposure resulted in several cases of incomplete development of the upper jaw, which had no observable effects on locomotion or survival but may impact the larvae's ability to feed in long-term scenarios (Olsvik et al., 2021).

4.4 Effects of plastic leachates on heart rate

The heart is one of the first organs to form during embryogenesis and is particularly vulnerable to environmental stressors, making abnormal heart rates an important indicator of developmental toxicity (Chen et al., 2022). The heart rate was measured on days 4, 6, 8, and 10 to gain a comprehensive understanding of cardiac development from fertilization to hatching. Across all plastic types tested, heart rates were significantly reduced relative to controls on at least one day. Notably, all polymers induced bradycardia at the highest exposure concentration (5.0 ppm) on day 6.

Bradycardia in fish embryos is widely recognized as a biomarker of stress and impaired cardiac development, reflecting both physiological coping mechanisms and potential developmental disruption (Chen et al., 2020; Alboni et al., 2011). This defense mechanism allows marine medaka to survive in fluctuating conditions by optimizing oxygen use (Dong et al., 2014). Reductions in heart rate during embryonic development and heart formation can lead to abnormal heart development and have long-term consequences for survival and fitness (Huang et al., 2012; Reynolds et al., 2022). Our findings that exposure to plastic leachates led to consistent reductions in heart rate suggest that plastic leachates can disrupt normal cardiac function in marine medaka embryos. Previous studies have shown that exposure to PS microplastics and nanoplastics elicits a similar bradycardia response in fish embryos, including

417 marine medaka (Chen et al., 2020) and zebrafish (Persiani et al., 2023), even at very low
418 concentrations.

419 The strong reductions in heart rate observed in this study may be linked to the formation
420 of reactive oxygen species (ROS) during plastic degradation. Microplastics are known to
421 generate ROS, with free radicals forming on particle surfaces as they weather (Kadac-Czapska et
422 al., 2024). In fish, elevated ROS levels can cause oxidative damage and trigger toxicity
423 responses, and oxidative stress has been directly associated with altered cardiac function
424 (Chowdhury and Saikia, 2020). Our findings suggest that high concentrations of PC, PET, PS,
425 PP, and PE plastic leachates may induce bradycardia during early cardiac development, with
426 PET and PS leachates eliciting this response at concentrations as low as 0.1 ppm.

427 *4.5 Histological assessment of adult marine medaka*

428 No significant structural differences were detected in the gill tissues of adult marine
429 medaka between the control and treatment groups, but variations in liver morphology were
430 observed. Evidence of hepatocellular vacuolation was observed in the PE 0.1 and PC 0.1 ppm
431 treatment groups, a response commonly associated with cellular stress or injury that may disrupt
432 normal liver function (Nayak et al., 1996). Similar effects were seen in European sea bass
433 (Dicentrarchus labrax), where exposure to PE and PVC plastics significantly increased
434 hepatocyte vacuolation and altered liver morphology (Espinosa et al., 2019). Excess
435 accumulation of lipofuscin granules was also seen in the PE 0.1, PE 0.5, and PC 0.1 ppm
436 treatment groups. Lipofuscin is a pigment that accumulates naturally with age but can form
437 prematurely in cases of high oxidative stress and ROS accumulation (Baldensperger et al., 2024).
438 The presence of high amounts of lipofuscin observed in our young adult fish may indicate that
439 oxidative stress is inducing changes within the liver. A similar result was observed in C. elegans,

where exposure to PS-NPs induced the accumulation of lipofuscin, indicating cellular damage due to increased oxidative stress (Liu et al., 2020).

Our results suggest that a short, 16-day exposure to plastic leachates may cause low to moderate liver damage in adult marine medaka, although further analysis is needed to confirm concentration-dependent effects and trends among treatment groups.

4.6 Antioxidant defense system response

To determine oxidative stress levels and the status of antioxidant defense systems, the *sod* and *gpx* genes were selected for evaluation. These genes play an essential role in regulating ROS levels and the antioxidant system (Huang et al., 2023). Oxidative stress results from an imbalance in the production of free radicals and the body's ability to neutralize these radicals using the antioxidant defense system, which can lead to cellular damage and promote inflammatory processes (Skoryk & Horila, 2023). The *sod* gene is an important regulator of ROS, which includes superoxide and hydrogen peroxide. Excess hydrogen peroxide is typically converted into less reactive hydroxyl compounds by *gpx*. However, the accumulation of hydrogen peroxide may result in cellular damage (Mişe Yonar et al., 2014).

Our results show that *sod* and *gpx* expression in adult male marine medaka was significantly downregulated in all treatment groups, suggesting a broad suppression of the antioxidant defense system. Significant reductions in *gpx* expression indicate that exposure to low concentrations of PE and PC leachates may impair antioxidant systems and lead to harmful hydrogen peroxide accumulation (Ramírez-Duarte et al., 2017). High levels of ROS production combined with suppression of the antioxidant defense system may lead to high levels of oxidative stress, potentially resulting in lipid peroxidation and DNA damage (Chandimali et al.,

2025). Prolonged oxidative stress may also increase the susceptibility of organisms to disease and infections (Skoryk & Horila, 2023). In females, both SOD and GPx expression remained unchanged relative to the controls. This response suggests that females experienced neither activation nor inhibition of the antioxidant defense system under plastic leachate exposure. Studies have shown that females are less susceptible to oxidative stress due to the antioxidant properties of estrogens such as 17β-estradiol (E2), which may promote the expression of antioxidant enzymes (Hameed et al., 2023; Kander et al., 2017; Strehlow et al., 2003).

4.7 Xenobiotic metabolism response

To understand how plastic leachate exposure affected the *ahr* signaling pathway and detoxification systems, *ahr* and *cyp1a1* genes were chosen for evaluation. *Ahr* is a ligand-activated transcriptional factor that is essential for responding to environmental stressors and toxins (Kou et al., 2024). *Ahr* primarily responds to hydrophobic chemicals such as dioxins and polycyclic aromatic hydrocarbons (PAHs), where it binds to the toxin and moves into the nucleus, and is responsible for activating detoxification genes such as *cyp1a1*. The *cyp1a1* gene plays an essential role in metabolizing foreign chemicals, otherwise known as xenobiotics, which is an important step in removing toxins from the body (Delescluse et al., 2000). Through this detoxification process, *cyp1a1* may also generate ROS, which can lead to increased oxidative stress if left to accumulate (Stading et al., 2020).

C*yp1a1* expression in adult male marine medaka was unchanged in the PE 0.1 ppm and PE 0.5 ppm treatment groups and significantly downregulated in the PC 0.1 ppm treatment group. Downregulation of *cyp1a1* in the PC 0.1 ppm treatment group, combined with downregulation of *gpx*, may indicate low oxidative stress levels, although the suppression of *cyp1a1* can lead to toxin accumulation in some cases (Czekaj et al., 2005). In females, exposure

to PE leachates induced significant downregulation of *cyp1a1* expression in all treatment groups, indicating a suppression of the detoxification pathway. These results are supported by previous studies showing that *O. melastigma* embryos exposed to plastic leachates in saltwater had downregulated *cyp1a1* expression levels, disrupting the *ahr* pathway (Qiu et al., 2023).

In adult marine medaka females, exposure to PC leachates significantly upregulated the expression of *cyp1a1* in the PC 0.1 ppm treatment group, indicating activation of the detoxification response. The differences seen in *cyp1a1* expression between males and females exposed to the PC 0.1 ppm treatment group may be attributed to sex hormone modulation of the *ahr* - *cyp1a1* pathway. The downregulation of *cyp1a1* can be mediated by the presence of androgens, which are responsible for the development and functions of the male reproductive system (Monostory et al., 2009). Conversely, the presence of estrogen has been shown to play a role in *cyp1a1* induction, leading to crosstalk between the *ahr* signaling pathway and estrogen receptors (Monostory et al., 2009; Wihlén et al., 2009).

4.8 Inflammatory and immune system response

Il-1ß is a pro-inflammatory cytokine that is essential in responding to infection and injury and is known to activate a wide range of inflammatory response genes (Lopez-Castejon & Brough, 2011). In adult marine medaka females, *il-1ß* expression was significantly upregulated in the PC 0.1 ppm treatment group and significantly downregulated in the PE 0.1 ppm and 0.5 ppm treatment groups. In males, *il-1ß* expression was significantly downregulated in the PC 0.1 ppm treatment group. Upregulation of *il-1ß* typically indicates activation of the inflammatory response, as it induces nuclear factor-κB (*nf-κb*), which is a key regulator of immune and inflammatory responses (Liu et al., 2017).

Cox-2 is an inducible enzyme activated by *nf-κb* that plays a role in regulating pain and inflammation, regulating the inflammatory response of the cardiovascular system, and supporting normal heart development in fish (Dong et al., 2010; Huang et al., 2007; Simon, 1999). Additionally, inhibition of *cox-2* has been shown to disrupt heart valve development, altering ventricle morphology and valve geometry (Scherz et al., 2008). In males, *cox-2* expression was significantly downregulated in the PC 0.1 ppm treatment group and reduced by 65% and 55% in the PE 0.1 ppm and 0.5 ppm treatment groups, respectively. Downregulation of both *il-1ß* and *cox-2* in the male PC 0.1 ppm treatment group suggests suppression of the inflammatory response. It has been reported that suppression of immune system genes such as *il-1ß* and *nf-κb* may lead to the downregulation of *cox-2* (Surh et al., 2001). In females, *cox-2* expression remained unchanged relative to the control, despite upregulation of *il-1ß*. This response indicates partial or early-stage activation of the inflammatory system, as *il-1ß* is an early-response gene, while *cox-2* is activated downstream (Jung et al., 2003).

C3 is a crucial activator of the complement system, which is a cascade of proteins involved in innate immunity and the destruction of pathogens (Cho et al., 2016). Both males and females showed no significant changes to C3 expression.

4.9 Comparative toxicities of plastic polymer types

DOC analysis revealed that release rates were greatest for PE and PP nurdles, with PP exhibiting much higher release rates than all other polymer types (Table 1). These results are consistent with other studies examining the photodegradation rates of polymers, which show that virgin PE and PP plastics released significantly higher rates of DOC than virgin PS and PET plastics (Delre et al., 2023).

Analysis of degradation pathways has revealed that polymers release distinct compounds depending on their chemical composition. For example, low-temperature pyrolysis shows that HDPE and PP primarily produce alkenes, alkanes, and alcohols; PS mainly yields aromatic compounds and styrene monomers; and PC produces alkanes and phenolic compounds (Jiang et al., 2024). The photodegradation of PET has been shown to release terephthalic acid (TPA), which may induce inflammation and respiratory impairment (Ishihara et al., 2025). Differences in degradation products may help explain observed differences in toxicity. PE and PP leachates appeared to induce lower rates of developmental toxicity than PC, PET, and PS leachates, despite having higher release rates of DOC. Conversely, PC and PET exhibited greater rates of mortality and developmental deformities, despite having two of the lowest DOC release rates. These results support the idea that toxicity is not directly associated with the amount of DOC released, but rather with the specific products produced by each polymer during degradation.

PC, PET, and PS contain benzene rings in their chemical structures, whereas PP and PE do not. Our hatching, mortality, and deformity responses across treatment concentrations showed that PC and PET elicited similar toxicity responses in marine medaka embryos when compared to PP and PE. PS exposure induced responses more comparable to PC and PET exposure than those from the non-aromatic polymers. The aromatic rings present in PC, PET, and PS may contribute to toxicity, as they can be metabolized into reactive intermediates that generate ROS, leading to oxidative stress and cellular damage (Chatterjee & Snyder, 1991; Paul & Pal, 2024). Benzene exposure has also been shown to affect the activity of antioxidant enzymes, further exacerbating oxidative damage and cellular harm (Paul & Pal, 2024). During the photodegradation period, PC and PET degraded more readily than PS, which may explain the greater toxicity effects observed under PC and PET exposure. Although polymers containing

benzene rings are generally more resistant to degradation due to their structural stability (Yuan et al., 2023), their persistence in the environment increases the likelihood of toxic byproducts leaching into marine environments over time, making them potential long-term sources of chemical pollution.

5. Conclusion

Table S1. Primers for qPCR

Figure S1. Representative histological sections of the gills of adult marine medaka after 16 days of exposure to plastic leachates. A: Control; B: PE 0.1 ppm; C: PE 0.5 ppm; D: PC 0.1 ppm. PL: Primary lamella; SL: Secondary lamella; E: Erythrocytes; CS: Cartilaginous support. Scale bar = 20 µm.

Part III: Spectroscopic analysis of photo-induced leachate of five different types of plastic nurdles

Methods

Analytical Measurements

Fluorescence excitation–emission matrix (EEM) spectroscopy

Fluorescence excitation–emission matrix (EEM) spectra were acquired using a Shimadzu RF-6000 spectrofluorometer (Shimadzu, Japan). Excitation wavelengths were scanned from 200 to 400 nm with a step size of 5 nm, and emission wavelengths were recorded from 280 to 550 nm at 1 nm intervals. The scan speed was set to 6000 nm min^{-1}. Both excitation and emission slit widths were fixed at 10 nm, and detector sensitivity was set to low. Artificial seawater was measured as a procedural blank using the same acquisition parameters and was used for background correction and Raman normalization during subsequent data processing.

UV-Visible (UV-Vis) absorption spectroscopy

UV–Vis absorption spectra were measured using a UV spectrophotometer (UV-2600, Shimadzu, Japan) at the scanning wavelength range of 220–550 nm at 1 nm intervals at a medium scan speed. Measurements were performed in a quartz cuvette with an optical path length of 1 cm. The average absorbance value between 545 nm and 550 nm was subtracted from the spectrum for baseline correction. The resulting absorbance spectra were used for fluorescence inner-filter effects correction.

Data Analysis

EEM spectra pre-preprocessing

Data preprocessing consisted of the following steps:

1) Blank subtraction
   Fluorescence signals from the artificial seawater blank were subtracted from all sample EEMs to remove background contributions from the solvent and instrument.
2) Inner-filter effect (IFE) correction
   Inner-filter effects were corrected using sample-specific UV–Vis absorbance spectra, assuming a 1 cm optical path length. Absorbance values were used to account for attenuation of both excitation and emission light within the sample matrix.

3) Raman normalization

Fluorescence intensities were normalized to the Raman scatter peak of water. Specifically, the Raman signal was interpolated and integrated over the emission range of 371–428 nm at an excitation wavelength of 350 nm, and all EEMs were normalized to this Raman area to minimize instrumental drift and inter-measurement variability.

4) Scatter removal and interpolation

First- and second-order Rayleigh scattering as well as Raman scattering regions were removed from the EEMs. A ±10-25 nm exclusion window was applied around scatter bands, and the affected regions were reconstructed using two-dimensional B-spline interpolation. Notably, the scattering exclusion window would largely influence the final eem and data interpretation, which should be optimized for each eem spectra: large enough to remove the scattering effect but smaller enough not to remove the eem information for the samples (maybe can test whether we can treat the scattering information as a PARAFAC part and remove it).

Fluorescence indices and peak analysis

Several commonly used fluorescence indices were calculated to characterize the source and compositional features of dissolved organic matter. These included the fluorescence index (FI), biological index (BIX), and humification index (HIX). Before index calculation, EEMs were smoothed to reduce high-frequency noise. Additionally, five characteristic fluorescence peak regions were identified using the peak classification scheme proposed by Coble. Protein-like and humic-like fluorescence components were quantified based on their established excitation–emission wavelength domains.

$$FI = \frac{f_{em470}}{f_{em520}} \ (ex370)$$

where, f_{em470} is fluorescence intensity of emission wavelength of 470 nm, at excitation wavelength of 370 nm. The f_{em520} as above. The FI indicates the source of DOM, which is either: microbial derived (FI > 1.8) or terrestrially (FI < 1.2) (McKnight et al., 2001).

$$HIX = \frac{\sum f_{em435\text{-}480}}{\sum f_{em300\text{-}345}} \ (ex254)$$

where, $\sum f_{em435\text{-}480}$ is the peak area under the emission spectra of 435–480 nm, at excitation wavelength of 254 nm. The $\sum f_{300\text{-}345}$ as above. The HIX indicates the content of humic substance or extent of humification. Greater values indicate high extent of humification (Ohno, 2002; Zsolnay et al., 1999).

$$BIX = \frac{f_{em380}}{f_{em430}} \ (ex310)$$

where, f_{em380} is fluorescence intensity of emission wavelength of 380 nm, at excitation wavelength of 310 nm. The f_{em430} as above. The BIX indicates the contribution of albuminoidal and biological components (Parlanti et al., 2000; Wilson and Xenopoulos, 2008).

Principal component analysis (PCA) analysis of EEM spectra

PCA was applied to the preprocessed EEM dataset to characterize major patterns of spectral variation among samples. Each EEM matrix was unfolded into a one-dimensional vector, and all samples were assembled into a sample-by-variable matrix, where each variable corresponded to an individual excitation-emission wavelength pair. Variables containing missing values, non-finite values, or zero variance across samples were removed before analysis. The resulting dataset was mean-centered and scaled to unit variance, and PCA was performed in R using the prcomp function. Sample scores were used to evaluate clustering and separation among treatments, while loading values were used to identify the wavelength regions contributing most strongly to PC1 and PC2.

Parallel Factor Analysis (PARAFAC) analysis of EEM spectra

The corrected EEM dataset was subjected to PARAFAC to resolve independent fluorescent components. PARAFAC assumes that multiple samples contain a limited number of common fluorescent components, and that differences among samples mainly arise from variations in the relative contribution of these shared components. Accordingly, all samples are described by one common set of excitation and emission spectral profiles, while the sample

loading matrix (A matrix) directly represents the intensity of each resolved component (e.g., C1, C2, and C3) in individual samples. The objective of PARAFAC is to identify the minimum number of components, F, required to adequately explain the trilinear structure of the EEM dataset, i.e., each component is represented as one vector in the sample, excitation, and emission modes, and the measured fluorescence signal is expressed as the linear combination of these components.

$$X(i,j,k) = \sum_{f=1}^{F} a_{if}\, b_{jf} c_{kf} + e_{ijk}$$

Where i is the sample, j is the excitation wavelength, k is the emission wavelength, F is the number of components, a is the sample loading (concentration-like), b is the excitation loading, c is the emission loading, e is the residual error.

Model fitting was performed using non-negativity constraints in all three modes by default, with sample-wise normalization enabled (normalise = TRUE) to reduce the influence of absolute intensity differences among samples. To minimize convergence to local minima, each model was initialized with 50 random starts (nstart = 50), and the convergence criterion was set to ctol = 1 × 10^-8. Candidate PARAFAC models were first screened by comparing model fit and component structure. The percentage of explained variance (R^2) was used to evaluate model performance, and models with high explanatory power were considered preferable. Core consistency diagnostics (corcondia) were further calculated to assess whether the chosen component number was consistent with an acceptable trilinear structure; values greater than 40 were considered indicative of an acceptable model.

The final model was further validated using several complementary approaches. Residual EEMs were inspected to evaluate whether the model captured the major fluorescence structure; an acceptable model was expected to leave only weak, randomly distributed residuals, without strong structured hotspots. Residual plots were also used to check whether scatter removal and interpolation had been adequately performed. Split-half validation was carried out to test model robustness by fitting the same component number to independent subsets of the dataset. Model stability was evaluated visually by comparing the overlap of split-half component spectra and quantitatively using Tucker's congruence coefficients

(TCCs), where values greater than 0.95 were regarded as strong evidence for reproducible components. In addition, leverage analysis was performed to identify influential samples and wavelength regions and to assess whether individual samples disproportionately affected model structure.

After validation, the selected three-component PARAFAC model was used to extract the sample-mode scores (A), emission loadings (B), and excitation loadings (C). Sample-mode scores were exported for subsequent comparison with fluorescence indices and other sample properties. The chemical plausibility of the resolved components was further assessed by comparison with characteristic fluorescence regions and, where appropriate, by reference to the OpenFluor database.

Results

UV-Vis spectra analysis

The UV–Vis absorbance of plastic-derived dissolved organic matter (pDOM) was mainly distributed between 230–300 nm region, suggesting the generation of low-molecular-weight compounds with limited conjugation. Interestingly, the characteristic UV–Vis absorption bands gradually shifted toward longer wavelengths in the order of PE, PP, PS, PC, and PET. Among all polymers, the degradation products of PET exhibit a clear characteristic absorption peak at around 250 nm. This peak can be attributed to $\pi \rightarrow \pi^*$ transitions of aromatic structures, such as small-molecule aromatic esters or aromatic carboxylic acids. While the characteristic absorption of PE and PP is located mainly in shorter wavelengths, suggesting a relatively simple degradation product with a lower degree of conjugation, most likely aliphatic oxidized molecules. Compared with PE and PP, PS showed a clear signal around 250 nm, suggesting the presence of aromatic low-molecular-weight compounds. PC exhibited a distinct absorption band in the 230–245 nm region with a noticeable tail retained over 250–280 nm, indicating that its dissolved photoproducts contained a greater contribution from aromatic oxidized structures and/or carbonyl-containing aromatic fragments.

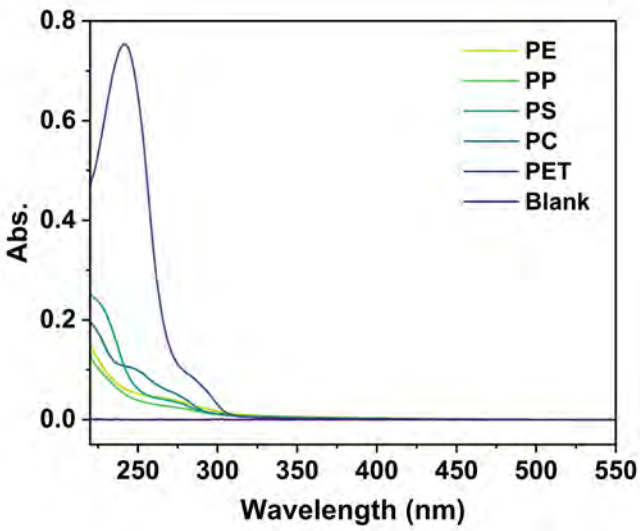

Figure 1: UV-Vis Spectra of the photo-induced leachate of different types of plastic nurdles

EEM spectra analysis

The EEM spectra and fluorescence indices of pDOM showed a clear increase in the aromaticity and conjugation degree in the order of PE < PP < PS < PC < PET, which is consistent with the UV – Vis absorption results. Among them, PET showed the most pronounced humic-like fluorescence signature, indicating the formation of highly oxidized and aromatic photoproducts.

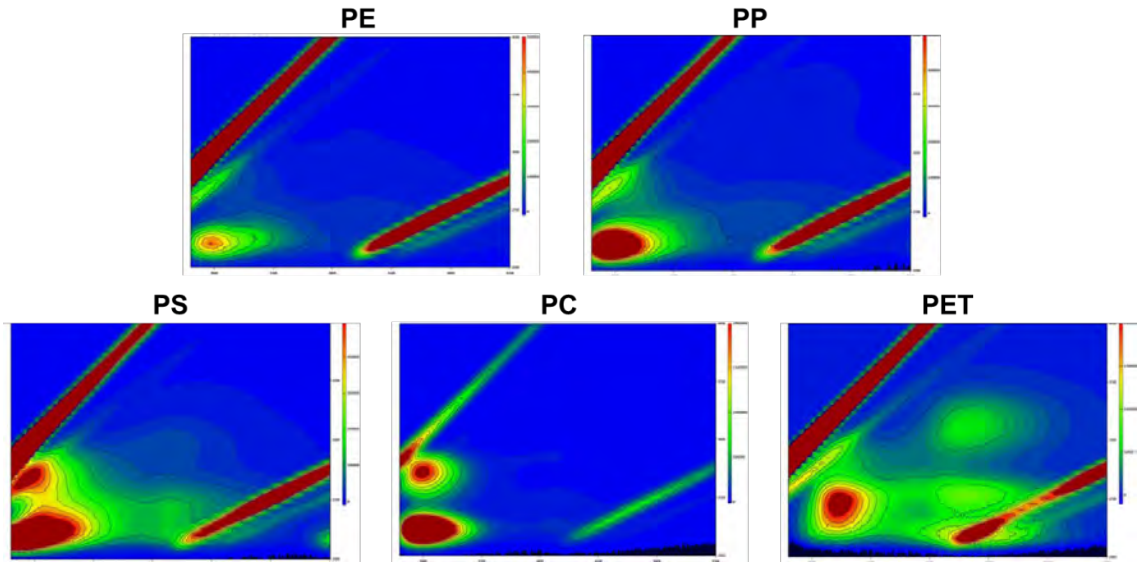

747 Figure 2: EEM Spectra of the photo-induced leachate of different types of plastic nurdles

748

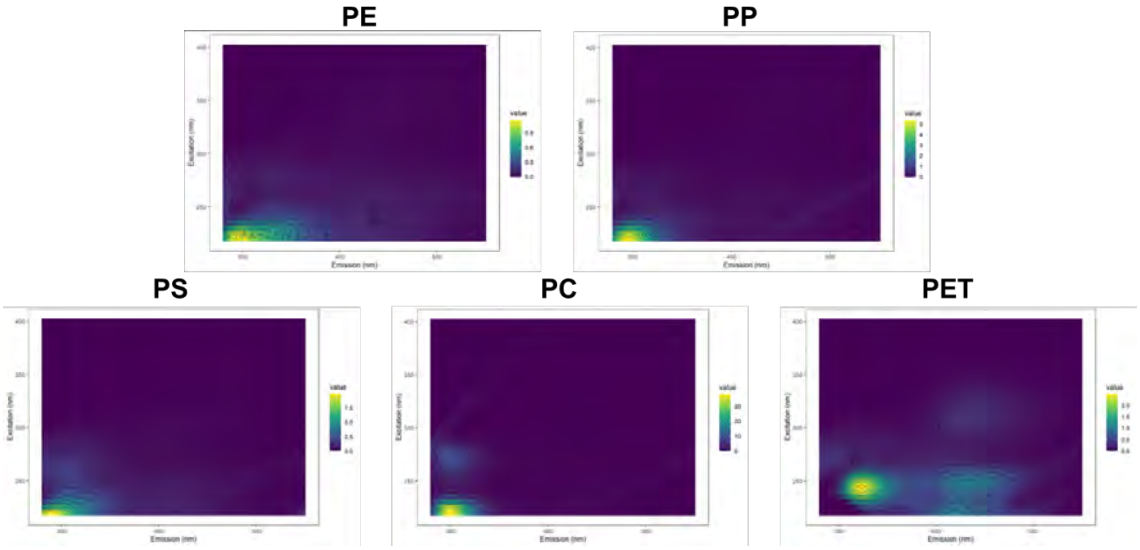

749

750 Figure 3: Corrected EEM Spectra of the photo-induced leachate of different types of plastic
751 nurdles

752

Plastics	Emission	Excitation	I_max
PE	302	220	1.16
PP	293	220	5.37
PS	288	220	9.97
PC	298	220	38.15
PET	324	245	2.49

753

754 Table 1: EEM Spectral peaks of the photo-induced leachate of different types of plastic
755 nurdles

Plastics	FI	BIX	HIX
PE	1.27	0.90	0.44
PP	1.10	0.85	0.33
PS	1.24	0.67	0.20
PC	1.09	0.69	0.07
PET	1.48	0.18	0.38

756

757 Table 2: Fluorescence indices of the photo-induced leachate of different types of plastic
758 nurdles

PCA analysis

PCA analysis showed that PC1 and PC2 mainly reflected differences between protein-like and humic-like fluorescence regions. PC1 mainly represented variation between long-emission humic-like fluorescence and some atypical scatter-related signals, whereas PC2 mainly distinguished changes between short-wavelength protein-like fluorescence and humic-like fluorescence. Specifically, the negative variation of PC2 was mainly associated with the region around Ex 230–235 nm / Em 281–287 nm, which is closer to the protein-like, especially tyrosine-like, fluorescence region, indicating that the negative direction of PC2 was related to short-emission protein-like signals. In contrast, the major positive contribution to PC2 was concentrated in the region around Ex 325–330 nm / Em 441–451 nm, which can be assigned to a typical humic-like fluorescence region and is close to the classical C peak, suggesting that the positive direction of PC2 mainly represented enhanced humic-like fluorescence. In addition, the long-emission region around Ex 220 nm / Em 487 nm also contributed positively to PC2, further supporting its association with humic-like signals.

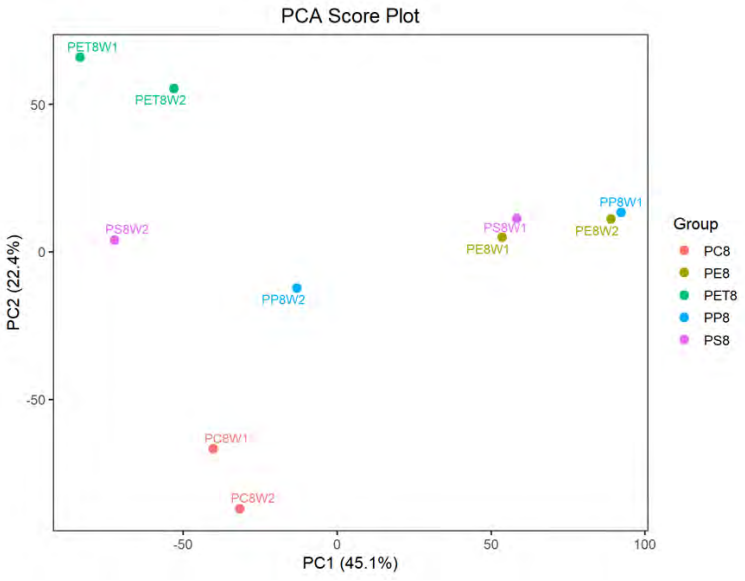

Figure 4: PCA plot of the EEM Spectra of the photo-induced leachate of different types of plastic nurdles

EEM-PARAFAC analysis

Model comparison

To determine the optimal number of PARAFAC components, model performance was evaluated by considering the percentage of the explained variance (R^2), core consistency diagnostic (corcondia), split-half validation, and residual analysis. Except for the two-component model, which showed an R^2 below 0.95, all other models yielded R values greater than 0.95 and did not exhibit a clear plateau. The CORCONDIA values for the two-, three-, four-, and higher-component models were 99, 62, 37, and 37, respectively. Corcondia values above 40 are generally considered to indicate an acceptable trilinear structure. Accordingly, both the two- and three-component models were deemed structurally acceptable. Based on the combined evaluation of R values and CORCONDIA, the three-component model was selected as the candidate optimal model for further validation.

Split-half analysis further supported the robustness of the three-component solution. As shown in Table 3, the majority of tcc_em and tcc_ex values for Comp.1, Comp.2, and Comp.3 were close to or greater than 0.95 across various split-half combinations, demonstrating highly consistent excitation and emission loadings for all three components. Overall, the three-component model accurately captured the key fluorescence fractions in the sample and was highly reproducible across independent data partitions. Overall, the three-component model reliably captured the major fluorescent fractions in the dataset and showed strong reproducibility across independent data partitions. Additionally, residual analysis also revealed good model performance. Except for the PC samples, which had small residual features in localized scatter regions and around the primary fluorescence peak due to their relatively high signal strength, residuals in the other samples were generally low and equally distributed. This suggests that the three-component model adequately explained the predominant fluorescence variability in the EEM dataset. Overall, the three-component PARAFAC model fit best for the decomposition of the EEM dataset.

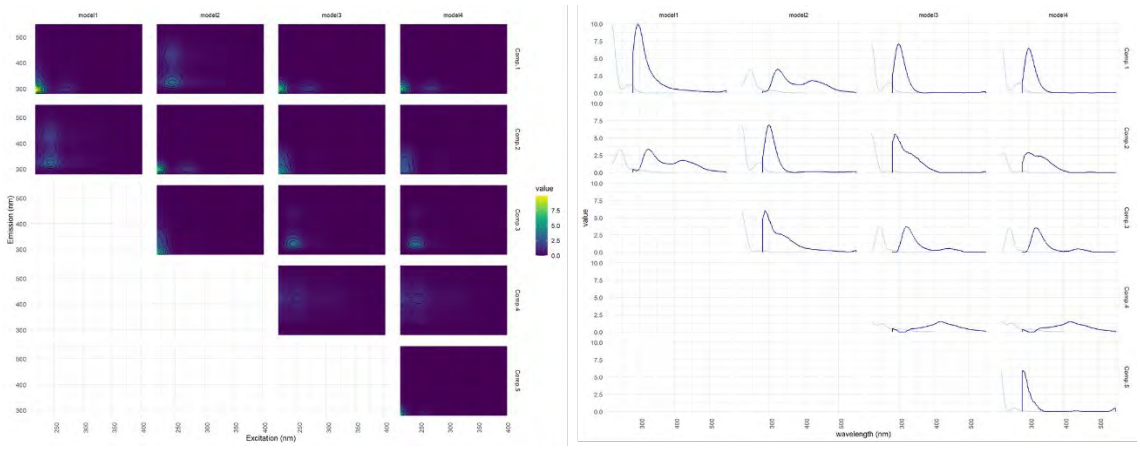

Figure 5: Different PARAFAC models (2-5 components) output showing the different fluorescent components (left) and the corresponding excitation/emission loadings (right)

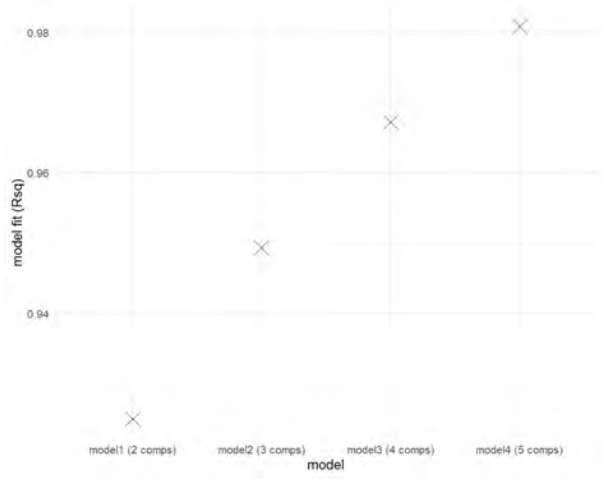

Figure 6: R^2 of different PARAFAC models (2-5 components) for model fit evaluation

Num.	component	comb	tcc_em	tcc_ex
1	Comp.1	ABvsCD	0.94	0.99
2	Comp.1	ACvsBD	1.00	0.99
3	Comp.1	ADvsBC	0.98	0.93
4	Comp.2	ABvsCD	0.83	0.88
5	Comp.2	ACvsBD	0.99	0.97
6	Comp.2	ADvsBC	1.00	1.00
7	Comp.3	ABvsCD	0.76	0.18
8	Comp.3	ACvsBD	1.00	1.00
9	Comp.3	ADvsBC	1.00	1.00

Table 3: TCC table of Three-component PARAFAC models for model evaluation

PARAFAC components

Three fluorescent components were identified in the EEM spectra of plastic-derived DOM. Component 1 showed excitation peaks at about 240 and 320 nm and an emission peak at 430 – 450 nm, indicating a humic-like substance. Component 2 had a main excitation peak at 220 – 230 nm and an emission peak around 300 nm, which is typical of tyrosine-like protein fluorescence. Component 3 showed excitation at 230 – 250 nm and emission at 320 – 340 nm, representing tryptophan-like or aromatic protein-like fluorescence. Based on the EEM features and fluorescence indices, polyolefins (PE and PP) were mainly characterized by protein-like components, while aromatic polymers (PS, PC, and PET) had higher proportions of tryptophan-like and humic-like components. PET showed the strongest humic-like signal, possibly related to secondary transformation under UV exposure.

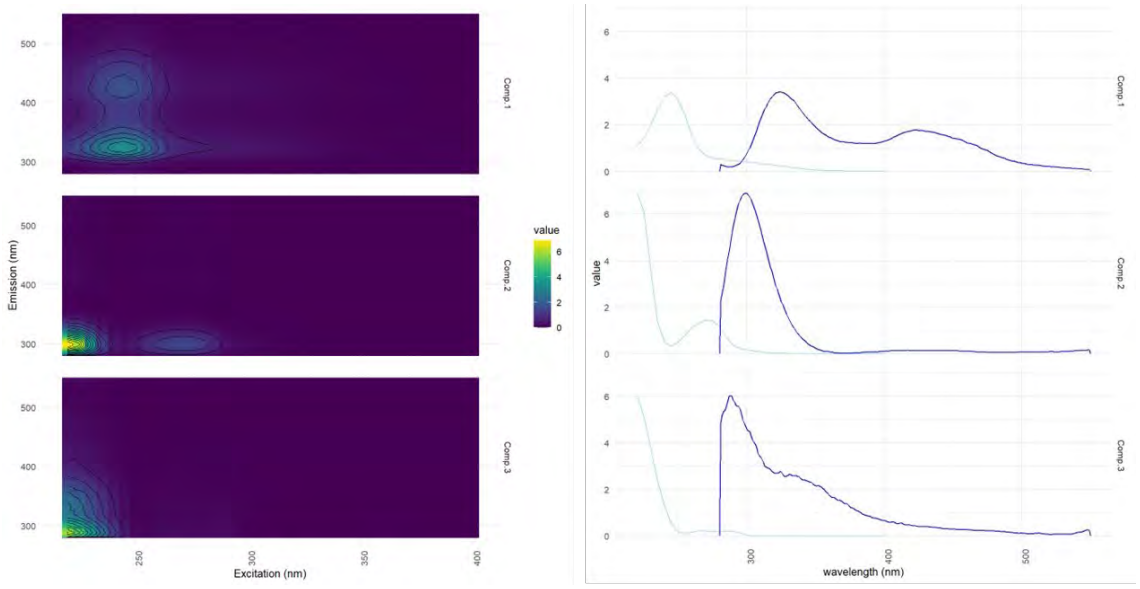

Figure 7: Three-component PARAFAC model output showing the different fluorescent components (left) and the corresponding excitation/emission loadings (right)

Component	Ex peak (nm)	Em peak (nm)	Assignments (Ref Cable peak)	Polymer type
C1	240 / 320	420–450	humic-like	PET
C2	225	300	protein-like (tyrosine-like)	PE, PP, PS
C3	230–250	320	tryptophan-like / aromatic protein-like	PS, PC

Table 4: Peaks of the fluorescent components of the three-component PARAFAC models and their assignments

Plastics	Comp.1	Comp.2	Comp.3
PE	2.26	2.12	8.93
PP	0.99	7.24	5.48
PS	2.17	6.20	5.48
PC	0.30	13.25	0.00
PET	6.79	0.00	0.00

Table 5: Fluorescent components loading of the three-component PARAFAC models

Discussions

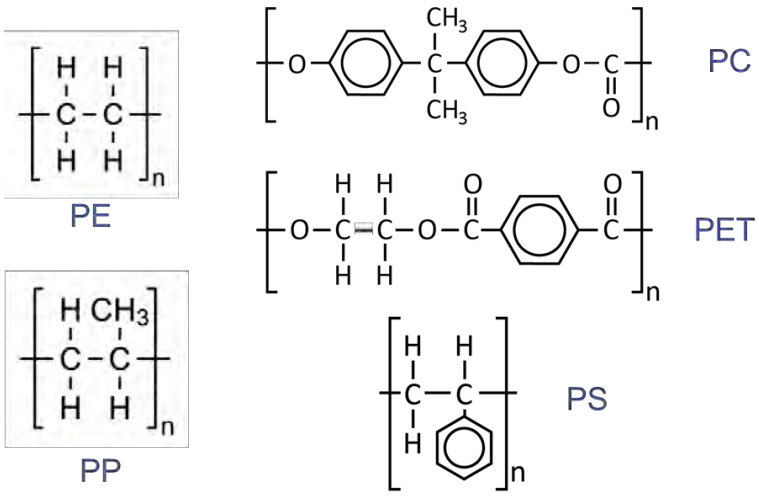

Figure 8: Structure of different types of plastic polymers

- DOC: PP＞PE＞PET＞PS＞PC
- Comprehensive toxicity: PE < PP < PS < PET < PC
- EEM max peak: PE < PET < PP < PS < PC
- PARAFAC loading:
  i. C1: PC < PP < PS < PE < PET
  ii. C2: PET < PE < PS < PP < PC
  iii. C3: PET = PC < PP = PS < PE

Next steps:

a) Calculate the Pearson correlation coefficient between Fmax values of individual fluorescent components in pDOC and toxicity values, for the discussion part.

b) Analyze the C/H ratios in pDOM using the LC-MS data (measured already).

c) Normalize the UV–Vis and EEM spectra to TOC.

d) Compare the PARAFAC components with the OpenFluor database.